International Journal of Robotics and Control Systems
Vol. 5, No. 6, 2025, pp. 3190-3207
ISSN 2775-2658
http://pubs2.ascee.org/index.php/ijrcs

Dynamics Evaluation of a PMSM Drive used for Residential Applications Employing Different Sensorless Techniques

Mahmoud A. Mossa [a,1,*], Hamid Chojaa [b,2], Alfian Ma'arif [c,3], Iswanto Suwarno [d,4]

[a] Electrical Engineering Department, Faculty of Engineering, Minia University 61111, Minia, Egypt
[b] Higher School of Technology, Industrial Technologies and Services Laboratory, Sidi Mohamed Ben Abdellah University, Fez 30000, Morocco
[c] Department of Electrical Engineering, Universitas Ahmad Dahlan, Yogyakarta, Indonesia
[d] Department of Electrical Engineering, Universitas Muhammadiyah Yogyakarta, Yogyakarta, Indonesia
[1] mahmoud_a_mossa@mu.edu.eg; [2] hamid.chojaa@usmba.ac.ma; [3] alfianmaarif@ee.uad.ac.id; [4] iswanto_te@umy.ac.id
* Corresponding Author

ARTICLE INFO

Article history
Received July 18, 2025
Revised August 19, 2025
Accepted December 22, 2025

Keywords
PMSM Drives;
Sensorless Control;
Dynamic Performance;
Residential Applications;
Estimation Error;
Robustness Test;
Comparative Study;
System Co-ordinates

ABSTRACT

The study concerns with evaluating the dynamic behaviour of a PMSM drive utilizing two distinct sensorless approaches. The evaluation process also considers the use of a load profile that emulates the torque of a compressor in a home refrigerator, i.e., simulating the coolant's compression and suction processes. The first sensorless method stands on comparing two stator voltage values in two different coordinates (real and hypothesis) to estimate the speed and position. Meanwhile the second method compares two current vectors expressed in the two coordinates to evaluate the speed signal. The two-coordinates are expressed in the direct-quadrature frame. To control the drive dynamics, a simple vector control scheme is adopted. The performance analysis is made easier by the presentation of the thorough mathematical derivations for each system component. Additionally, each sensorless scheme's theoretical base is thoroughly explained. The comparative analysis's aim is to highlight the differences between the two sensorless techniques over the considered operating conditions. The system's robustness and speed estimation error are used to provide the judgment. Additionally, a low-speed operating range is selected while applying the domestic load profile to illustrate the limitation of both senseless. The obtained results reveal and confirm the superiority of the current vector-based sensorless scheme via achieving lower estimation error and better system robustness against model uncertainties. Statistically, the sensitivity of the current-variant based recorded a reduction of 37.5%, 55.175 and 99.8% of the sensitivity of the voltage variant based, when considering respectively a change of 30% of stator resistance, stator inductance and permanent flux.

1. Introduction

Permanent magnet synchronous motors (PMSMs) have become increasingly prominent in modern drive applications due to their high efficiency, compact size, and wide operating speed range [1]–[4]. In high-performance applications such as robotics, machine tools, and advanced residential

appliances, precise speed and torque control is required under dynamic conditions and parameter variations [5]–[9]. The adoption of vector control enables PMSM drives to emulate the performance of separately excited DC motors by independently regulating torque and flux components [10]–[15]. However, such high-performance control relies on accurate knowledge of rotor position and speed, typically obtained from physical sensors. The reliance on sensors introduces additional cost, reduced reliability, and sensitivity to harsh environments, motivating widespread research into sensorless control strategies for PMSM drives [18]–[23].

Traditional proportional-integral (PI) controllers dominate PMSM drive implementations because of their simplicity, but they exhibit poor robustness under parameter variations, disturbance, or nonlinear saturation effects [11], [16], [17]. Accurate regulator tuning becomes more challenging across wide speed ranges, especially if model-based conditions and real-time constraints are not met. Consequently, advanced observer-based and model-reference sensorless strategies have been proposed to estimate rotor speed and position while reducing dependence on direct sensing, offering enhanced reliability and reduced cost [24]–[27].

Several sensorless estimation techniques have been reported in the literature, each with distinct advantages and limitations. The Extended Kalman Filter (EKF) is widely used for its noise filtering and adaptive capability, yet it involves significant computational burden [31]. Model Reference Adaptive Systems (MRAS) offer simplicity but are sensitive to parameter drift [27]–[29], while Sliding Mode Observers (SMO) and full-order flux observers are praised for robustness but often suffer from chattering and require tuning of switching gains [32]–[34]. Phase-Locked Loop (PLL) and Second-Order Generalized Integrator (SOGI)-based observers have also gained attention for improved low-speed performance [33]–[35]. Disturbance-Observer-Based (DOB) and Integral State Feedback observers enhance disturbance rejection but often rely on assumptions such as constant speed or known load torque [36]–[38]. Most prior studies focus on performance within specific speed regions or under constant or lightly varying loads, without a comprehensive comparative framework that considers computational complexity, noise sensitivity, robustness, and practical applicability simultaneously. These assumptions limit the practical applicability of such observers unless compensatory mechanisms are integrated. Therefore, a detailed and comparative evaluation of existing sensorless observers is required to highlight these limitations under realistic operating scenarios.

Existing sensorless techniques for PMSM drives vary not only by estimation mechanism but also by computational complexity, noise sensitivity, and robustness to parameter variations. These approaches can be broadly characterized as observer-based estimation utilizing integration of speed signals [25]–[27] and methods relying on differentiation of estimated position signals [30]–[35]. However, each category involves trade-offs: integration-based observers may suffer from drift and steady-state errors in low-speed regions, whereas differentiation-based methods are heavily affected by noise, resulting in imprecise estimates. Beyond these two traditional categories, hybrid and disturbance-observer-based techniques have also emerged, with diverse performance in terms of convergence speed, real-time implementation feasibility, and compatibility with varying load conditions [36]–[39]. A comprehensive assessment of these multidimensional criteria—such as estimation accuracy, robustness, computational burden, and adaptability to load variations—is still lacking in the literature.

Although PMSM sensorless control has been extensively addressed for industrial and automotive systems, fewer studies explicitly examine performance under residential load profiles where load dynamics may differ due to intermittent and nonlinear loads—such as refrigerator compressors or household appliances. These conditions present unique challenges concerning low-speed operation, torque pulsations, and transient load steps. The motivation for the present study lies in bridging this research gap by evaluating multiple sensorless estimation schemes of a PMSM under a practical residential operating scenario, incorporating a realistic compressor torque profile.

The main study contributions can be thus itemized as follows:

- The dynamic behavior of a PMSM drive is analyzed while adopting different sensorless techniques with a residential load profile.
- Detailed mathematical analysis for the considered control and sensorless systems is presented to clarify the theoretical base of each topology.
- A torque profile of a refrigerator's compressor is adopted to emulate the operation of the sensorless schemes for residential uses.
- The comparative investigation made it possible to determine each sensorless scheme's advantages and disadvantages.

The following is how the paper is structured: The adopted control and system modeling are introduced in Section 2 and Section 3. A thorough theoretical analysis of the sensorless methods under study is presented in Section 4. Subsequently, Section 5 presents an evaluation of the drive performance under each sensorless technique while applying the residential load. Lastly, the study's conclusions are presented in Section 6.

2. PMSM model

Fig. 1 shows the per phase equivalent circuit of PMSM. Additionally, the PMSM's electrical and mechanical sub-models can be represented using the subsequent expressions defined in d-q co-ordinates [11]:

$$\frac{di_{ds}}{dt} = \frac{1}{L_s}(u_{ds} - R_s i_{ds} + \lambda_{qs}\omega_{me}) \tag{1}$$

$$\frac{di_{qs}}{dt} = \frac{1}{L_s}(u_{qs} - R_s i_{qs} - \lambda_{ds}\omega_{me}) \tag{2}$$

$$\frac{d\omega_{me}}{dt} = \frac{1}{J_m}(T_e - T_l - F\omega_{me}) \tag{3}$$

where R_s and L_s are the stator resistance and inductance; λ_{ds} and λ_{qs} are the d-q components of stator flux; ω_{me} is the electrical rotor speed; u_{ds}, u_{qs} and i_{ds}, i_{qs} are the d-q components of stator voltage and current, respectively. The symbols T_e and T_l refer to the electromagnetic and load torques, while J_m and F refer to rotor's inertia and friction constant.

The developed motor torque can be expressed by,

$$T_e = 1.5P\lambda_{mg}i_{qs} \tag{4}$$

where λ_{mg} is rotor flux and P is the pole pairs.

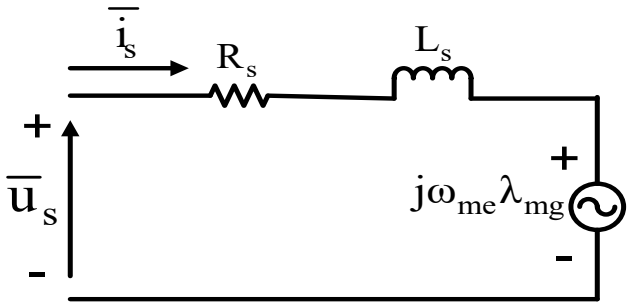

Fig. 1. Equivalent circuit model of PMSM

3. Adopted Control System

It is worth notifying that the main purpose of presented study is to evaluate the dynamics of PMSM under different sensorless techniques while applying a load torque emulating a residential load profile. Accordingly, adopting the vector control can be considered sufficient to maintain a prescribed speed and torque references.

The primary goal of this control is to completely align the rotor flux with the stator's direct axis in order to accomplish the following equality

$$\lambda_{ds} = \lambda_{mg} \tag{5}$$

The aforementioned relationship is achieved by keeping i_{ds} equal to zero. In order to maintain the flux inside the motor at the proper rate, this operation is typically utilized to avoid field weakening.

Consequently, by adjusting the current i_{qs} in accordance with (4), the motor's torque can be easily managed. The schematic diagram of vector controlled PMSM driving a compressor's load is shown in Fig. 4. It is observed that in order to guarantee accurate transformation between various coordinates, both the rotor's speed (ω_{me}) and position (θ_{me}) must be precisely identified. Therefore, one of the most important tasks to do is to investigate the proper sensorless scheme. As will be stated later, two distinct sensorless schemes are used to evaluate the dynamic performance of the PMSM drive under different operating conditions.

The main operation of the control depends on the tuning of the two PI current controllers that provide the reference voltages. The tuning process can be simply accomplished via aligning the poles of the linear PI regulators with that of the second order dynamic system [40]. This is to ensure the stability via achieving reasonable settling and fast damping. The mathematical analysis for tuning PI current regulators is accomplished as follows.

The relationships (1) and (2), can be represented by

$$u_{ds} = \overbrace{(R_s i_{ds} + L_s \frac{di_{ds}}{dt}}^{active\ part} - \overbrace{L_s \omega_{me} i_{qs}}^{compensating\ part}) \tag{6}$$

$$u_{qs} = \overbrace{R_s i_{qs} + L_s \frac{di_{qs}}{dt}}^{active\ part} + \overbrace{L_s \omega_{me} i_{ds} + \omega_{me} \lambda_{mg}}^{compensating\ part} \tag{7}$$

The compensating parts are used to reduce disturbances, while the active parts are used to drive the transfer function, which controls how the stator voltage will respond to changes in the stator current, and produce the required change in the stator current. The active terms are then subjected to the Laplace transform, which yields

$$\begin{aligned} u_{ds}(s) &= (sL_s + R_s) i_{ds}(s) \\ u_{qs}(s) &= (sL_s + R_s) i_{qs}(s) \end{aligned} \tag{8}$$

By arranging (8), it gives

$$\frac{i_{ds}(s)}{u_{ds}(s)} = \frac{i_{qs}(s)}{u_{qs}(s)} = \frac{1}{SL_s + R_s} \tag{9}$$

Additionally, the PI current regulators' transfer function is depicted by (10) and (11).

$$u_{ds}(s) = (k_p + \frac{K_i}{s}) * (i_{ds}^*(s) - i_{ds}(s)) \tag{10}$$

$$u_{qs}(s) = (k_p + \frac{K_i}{s}) * (i^*_{qs}(s) - i_{qs}(s)) \tag{11}$$

By replacing the voltage components $u_{ds}(s)$ and $u_{qs}(s)$ from (6) and (7), and after some mathematical derivations, the following expressions are obtained:

$$\begin{aligned} \frac{i_{ds}(s)}{i^*_{ds}(s)} &= \frac{sK_p + K_i}{s^2L_s + s(R_s + K_p) + K_i} \\ \frac{i_{qs}(s)}{i^*_{qs}(s)} &= \frac{sK_p + K_i}{s^2L_s + s(R_s + K_p) + K_i} \end{aligned} \tag{12}$$

The characteristic equation governing the dynamics of the PI current regulators is represented by the denominator of (12); for the system to remain stable, the denominator must have negative real roots. Consequently,

$$s^2L_s + s(R_s + K_p) + K_i = 0 \tag{13}$$

The expression (13) is a second order dynamic system, and to make it stable, it must align with the characteristic equation of the general second-order system expressed by

$$s^2 + 2\mathcal{E}w_c s + w_c^2 = 0.0 \tag{14}$$

where $\mathcal{E}$ and w_c are the damping factor and system's natural frequency, respectively.

Accordingly, by comparing the terms of (13) and (14), the tuned PI coefficients are determined as

$$\begin{aligned} K_p &= 2\mathcal{E}w_c - R_s \\ K_i &= w_c^2 L_s \end{aligned} \tag{15}$$

To testify the correctness of the tuning procedure, a bode plot for the transfer function of (12) using the tuned values is presented in Fig. 2, which reports that the system is stable.

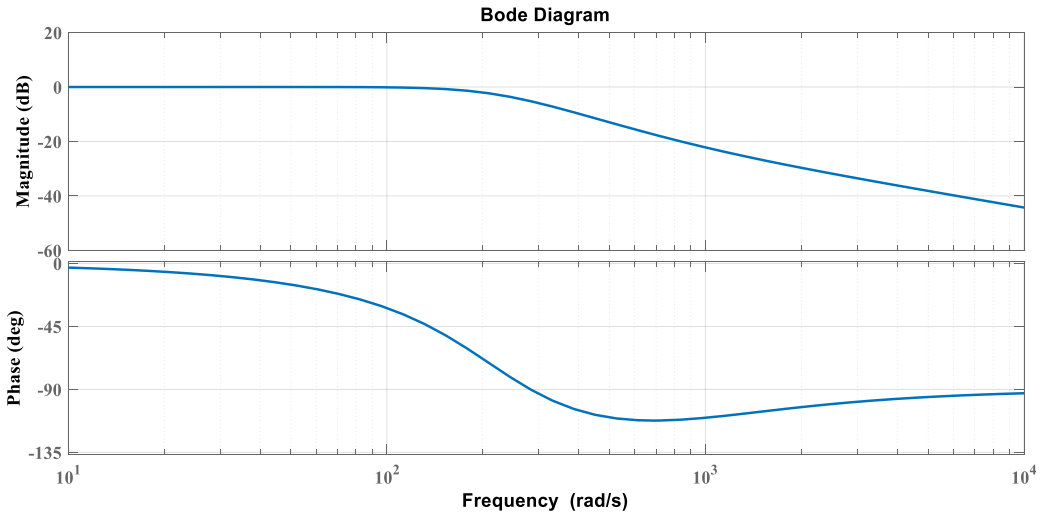

Fig. 2. Bode plot of PI regulator's transfer function

4. Adopted Sensorless Schemes

4.1. Voltage Variant-Based Sensorless

This method compares the value of stator voltage vector in two reference systems, one presumptive and one real, to provide a signal proportional to the speed and rotor position. As shown in Fig. 3, two co-ordinate systems—the d-q and γ-δ axes—are introduced in the model. The d-axis is aligned with the rotor flux (λ_{mg}), and the d-q axes are typically used to define the actual rotor position. Alternatively, a hypothetical co-ordinate system is represented by the γ-δ axes, creating a position difference of Δθ between the two co-ordinates defined as follows.

$$\Delta\theta = \theta_c - \theta_{me} \tag{16}$$

where θ_{me} and θ_c are the real and presumptive rotor positions.

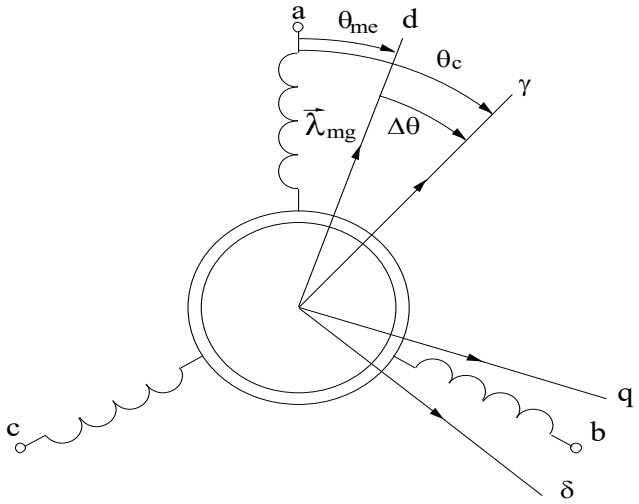

Fig. 3. Real and hypothetical frames

From Fig. 4, the voltage components represented in the γ-δ presumptive frame are expressed by

$$\begin{bmatrix} u_\gamma \\ u_\delta \end{bmatrix} = \begin{bmatrix} R_s + pL_s & -L_s\omega_c \\ L_s\omega_c & R_s + pL_s \end{bmatrix} \begin{bmatrix} i_\gamma \\ i_\delta \end{bmatrix} + \lambda_{mg}\omega_{me} \begin{bmatrix} -sin\,(\Delta\theta) \\ cos\,(\Delta\theta) \end{bmatrix} \tag{17}$$

The estimated position and speed can be obtained via considering ideal space vector allocation ($\Delta\theta = 0$ and $\omega_c = \omega_{me}$), which gives

$$\begin{bmatrix} u'_\gamma \\ u'_\delta \end{bmatrix} = \begin{bmatrix} R_s + pL_s & -L_s\omega_c \\ L_s\omega_c & R_s + pL_s \end{bmatrix} \begin{bmatrix} i_\gamma \\ i_\delta \end{bmatrix} + \lambda_{mg}\omega_{me} \begin{bmatrix} 0 \\ 1 \end{bmatrix} \tag{18}$$

where u'_γ and u'_δ represent the estimated voltage terms along the γ-δ axes.

The formulae in (18) represented the estimated voltages in the d-q frame considering zero displacement between the two co-ordinates (real and presumptive). As can be noticed the voltage difference along the γ-axis can be utilized to estimate the rotor position, accordingly

$$\Delta u_\gamma = u_\gamma - u'_\gamma = \lambda_{mg}\,\omega_{me}\;sin\,(\Delta\theta) \tag{19}$$

Via assuming $\Delta\theta$ being very small, then the position difference $\Delta\theta$ can be evaluated directly using the voltage difference along the γ-axis as

$$\Delta u_\gamma = u_\gamma - u'_\gamma \propto \Delta\theta \tag{20}$$

After estimating the displacement $\Delta\theta$, the successive task is to synchronize the two co-ordinates (real and presumptive). This can be done via reducing the rotating speed of the presumptive axis when $\Delta\theta > 0$ and increasing the speed when $\Delta\theta < 0$ as indicated in Fig. 4 which outlines the synchronizing procedure.

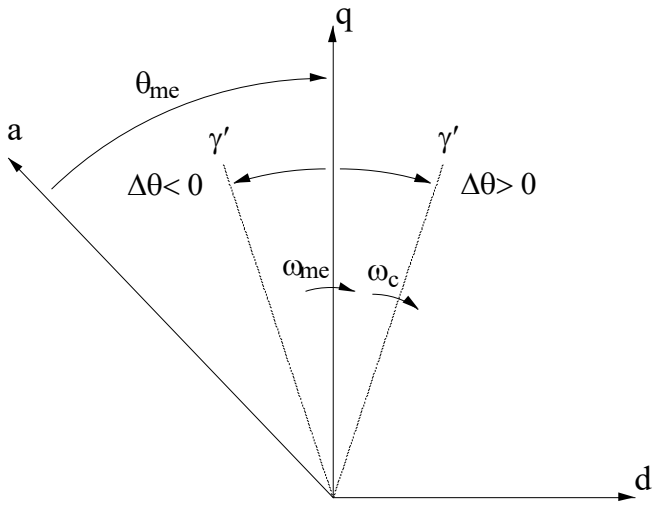

Fig. 4. Self synchronizing procedure

Estimating the reference system's rotational speed is essential to achieving this synchronization. The δ component of (18) makes it simple to get this estimate:

$$\omega_{me} = \frac{u_\delta - (R_s + L_s p) i_\delta}{\lambda_{mg} + L_s i_\gamma} \tag{21}$$

As the position is obtained via integrating the speed, the displacement $\Delta\theta$ can be minimized via adapting a speed correction factor α. This factor thus pertains to the error between the speed of presumptive and real co-ordinates.

$$\alpha = \omega_c - \omega_{me} \tag{22}$$

These factors allow for the development of an algorithm that, in the event of clockwise or counterclockwise rotation, acts on α and moves $\Delta\theta$ towards zero. Accordingly, the value of correcting factor α can be evaluated with the help of a PI regulator as follows

$$\alpha = -\left(K_{sp}\Delta u_\gamma + K_{si}\int \Delta u_\gamma dt\right) sgn(\omega_c) \tag{23}$$

where K_{sp} and K_{si} are the used corrective PI gains.

By appropriately correcting the estimation using the α factor, the rotor speed can be estimated as follows:

$$\omega_c = \omega_{me} + \alpha \tag{24}$$

where ω_{me} is evaluated using (11).

The overall sensorless vector-controlled scheme can now be constructed as shown in Fig. 5.

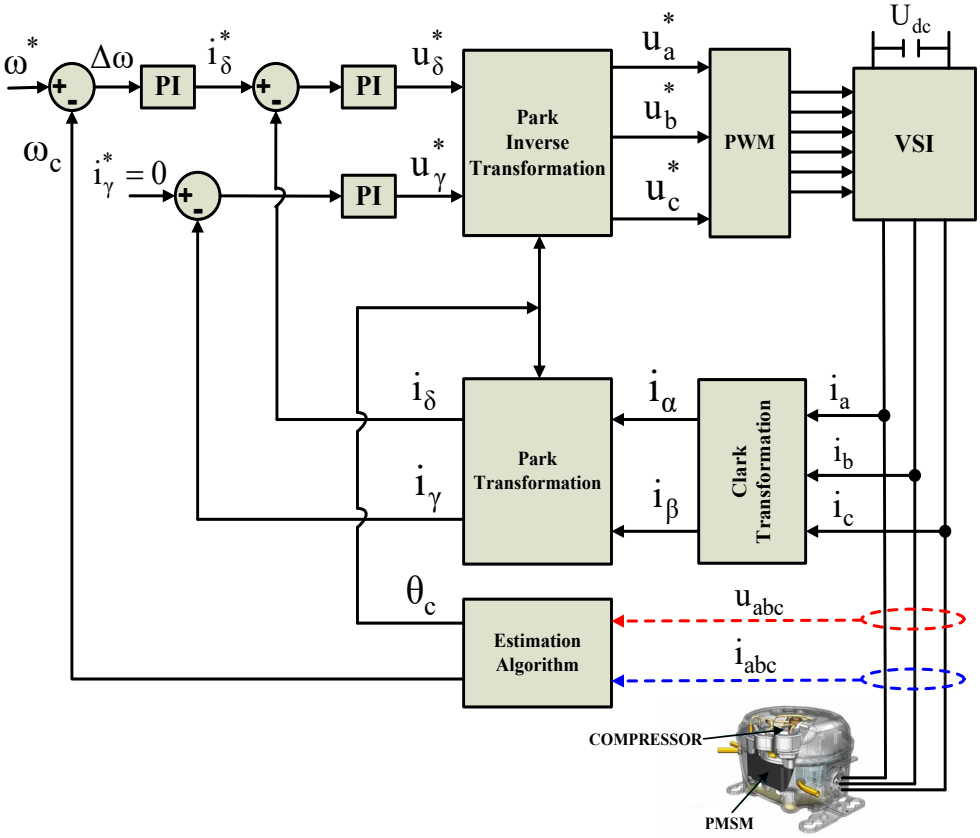

Fig. 5. Schematic diagram of first sensorless approach of PMSM drive

4.2. Current variant-based sensorless

By using the current as a state vector instead of the voltage, this method adds a minor variation to the sensorless scheme while maintaining the core idea of the previously described approach in (4.1). The algorithm compares the current evaluated by manipulating the PMSM equations in the γ-δ frame with the decomposed actual current along the d-q frame, taking into account the factors outlined in the preceding approach in (4.1).

It is possible to express the dynamics of the presumptive γ-δ currents as follows:

$$p\begin{bmatrix} i_\gamma \\ i_\delta \end{bmatrix} = \frac{1}{L_s}\left[\begin{bmatrix} u_\gamma \\ u_\delta \end{bmatrix} - \begin{bmatrix} R_s & -L_s\omega_c \\ L_s\omega_c & R_s \end{bmatrix}\begin{bmatrix} i_\gamma \\ i_\delta \end{bmatrix} - \lambda_{mg}\omega_{me}\begin{bmatrix} -\sin(\Delta\theta) \\ \cos(\Delta\theta) \end{bmatrix}\right] = \frac{1}{L_s}\left[\begin{bmatrix} u_\gamma \\ u_\delta \end{bmatrix} - \begin{bmatrix} R_s & -L_s\omega_c \\ L_s\omega_c & R_s \end{bmatrix}\begin{bmatrix} i_\gamma \\ i_\delta \end{bmatrix} - e\begin{bmatrix} -\sin(\Delta\theta) \\ \cos(\Delta\theta) \end{bmatrix}\right] \tag{25}$$

where e pertains to the electro-motive force.

By presenting the currents at a given instant as i_γ^n and i_δ^n, then the currents at the next sampling instant i_γ^{n+1} and i_δ^{n+1} can be evaluated by

$$\begin{bmatrix} i_\gamma^{n+1} \\ i_\delta^{n+1} \end{bmatrix} = \begin{bmatrix} i_\gamma^n \\ i_\delta^n \end{bmatrix} + p\begin{bmatrix} i_\gamma \\ i_\delta \end{bmatrix}T \tag{26}$$

The expressions of real system can be formulated assuming that the sampling period (T) is substantially lower than the stator current time constant. An essential presumption is that the two reference systems (real and presumptive) are aligned, have the same angular velocity ($\omega_c = \omega_{me}$),

and have no angular displacement ($\Delta\theta = 0$). According to this hypothesis, the formulae (25) and (26) are represented by

$$p\begin{bmatrix} i_\gamma'^{,n} \\ i_\delta'^{,n} \end{bmatrix} = \frac{1}{L_s}\left[\begin{bmatrix} u_\gamma \\ u_\delta \end{bmatrix} - \begin{bmatrix} R_s & -L_s\omega_c \\ L_s\omega_c & R_s \end{bmatrix}\begin{bmatrix} i_\gamma \\ i_\delta \end{bmatrix} - e_c\begin{bmatrix} 0 \\ 1 \end{bmatrix}\right] \tag{27}$$

$$\begin{bmatrix} i_\gamma'^{,n+1} \\ i_\delta'^{,n+1} \end{bmatrix} = \begin{bmatrix} i_\gamma'^{,n} \\ i_\delta'^{,n} \end{bmatrix} + p\begin{bmatrix} i_\gamma \\ i_\delta \end{bmatrix}T \tag{28}$$

In this case, e_c stands for the motor's emf in the new frame. The sensorless technique compares currents in the two different frames to obtain the estimated speed value.

By comparing (26) and (28), and assuming very small sampling interval, one can obtain the deviation between the actual sensed currents and those that were computed using the system model as follows

$$\begin{bmatrix} \Delta i_\gamma'^{,n+1} \\ \Delta i_\delta'^{,n+1} \end{bmatrix} = \begin{bmatrix} i_\gamma^{n+1} - i_\gamma'^{,n+1} \\ i_\delta^{n+1} - i_\delta'^{,n+1} \end{bmatrix} = \frac{T}{L_s}\begin{bmatrix} e.\Delta\theta \\ -(e - e_c) \end{bmatrix} \tag{29}$$

It is obvious from (29) that the position information can be derived utilizing the current deviation along the γ-axis. After some manipulation, the estimated position is evaluated by

$$\theta_c^{n+1} = \theta_{cn} + \frac{e_c^{n+1}}{\lambda_{mg}}T + K_e \cdot \Delta i_\gamma^n \tag{30}$$

Consequently, the speed can be estimated by differentiating (30), which gives

$$\omega_c^{n+1} = \frac{\theta_c^{n+1} - \theta_c^n}{T} = \frac{e_c^{n+1}}{\lambda_{mg}} + \frac{K_\theta}{T} \cdot \Delta i_\gamma^n \tag{31}$$

K_θ and K_e are gains in these formulations, and their values are modified to produce the intended results. Deviations in voltage and current are both essential to solving the sensorless drive issue. Interestingly, this technique has the benefit of utilizing lower voltage terms, which successfully reduces the uncertainty brought on by the inverter.

The sensorless approach discussed in this part is implemented in a systematic manner, as summarized in Fig. 6. Observably, two distinct current signals are recorded (measured and estimated), compared, and the error is then sent to the estimator, which yields the observed speed signal.

5. Performance Evaluation and Discussion

To investigate the sensitivity of the two prescribed sensorless schemes to changes in the model parameters (R_s, L_s and λ_{mg}), numerous tests are conducted. The obtained results show that the current variant based sensorless technique outperforms the performance of other voltage variant based approach through exhibiting low sensitivity levels to the parameters variation. The tests also considered the application of a load profile that emulates the torque of a compressor in a domestic refrigerator (i.e. emulating the compression and suction of the coolant). The obtained results from these loading conditions illustrate the superiority of the current variant based sensorless technique in maintaining the reference speed with minimum torque oscillations.

In this regard, parametric sensitivity is defined of the speed as parameter G varies of the machine (naturally the considerations are made at full speed) as follows:

$$S_{\omega}^{G} = \frac{\frac{\Delta\omega}{\omega_{actual}}}{\frac{\Delta G}{G}} \tag{32}$$

By varying the speed and imposing in turn a variation of approximately 30% on the parameters inserted in the equations, hyperbolic curves are obtained which provide a further verification of the limit of the operating range of the method in analyses. In fact, as the speed decreases, the sensitivity increases dramatically, thus making this method unusable below this value.

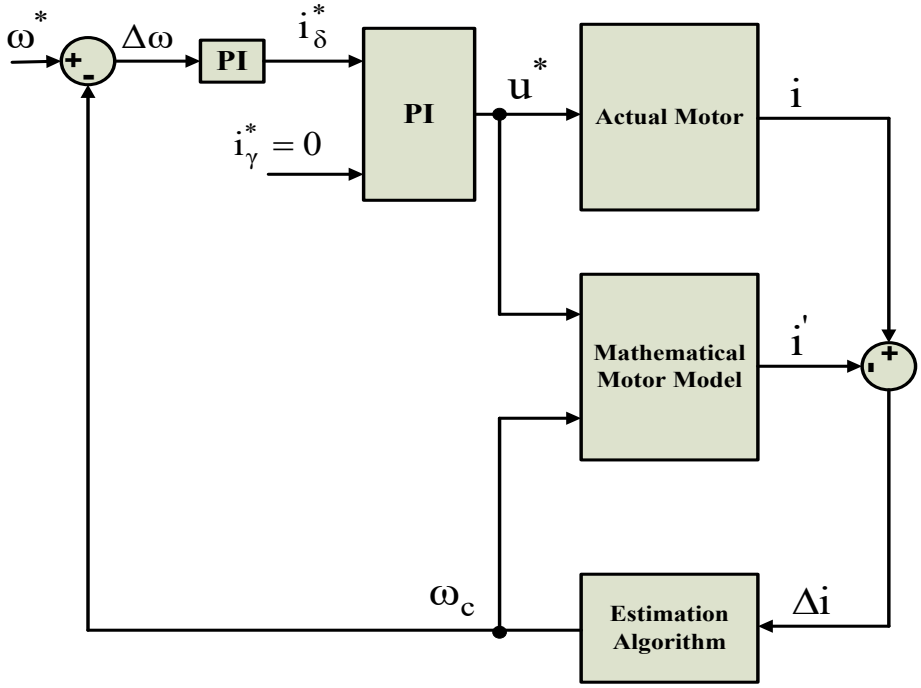

Fig. 6. Current vector based sensorless scheme

Fig. 7–Fig. 12 are the illustrations of the parametric sensitivities obtained from the tests carried out on the two adopted sensorless approaches. By comparing Fig. 7, Fig. 8 and Fig. 9, where the behaviours of $S_{\omega}^{R_s}$, $S_{\omega}^{L_s}$ and $S_{\omega}^{\lambda_{mg}}$ obtained from the voltage variant are reported, with Fig. 10, Fig. 11 and Fig. 12, of the current variant, there is a notable difference in behavior between the two. In particular it cannot ignore the remarkable difference existing between the two figures reporting the behaviour of $S_{\omega}^{\lambda_{mg}}$. This can be explained by observing (29)–(31) which allows the value of the counter EMF to be corrected at each interval, thus compensating for any variations in the parameter. These graphs therefore help to further highlight the better functioning of the second variant sensorless technique (current based) in terms of robustness. The recorded sensitivity impact can be briefed in Table 1.

Table 1. Sensitivity levels for the two adopted sensorless schemes

Adopted method	Sensitivity to changes in:		
	R_s	L_s	λ_{mg}
Current variant	1.2	3.2	0.01
Voltage variant	3.2	5.8	6.8

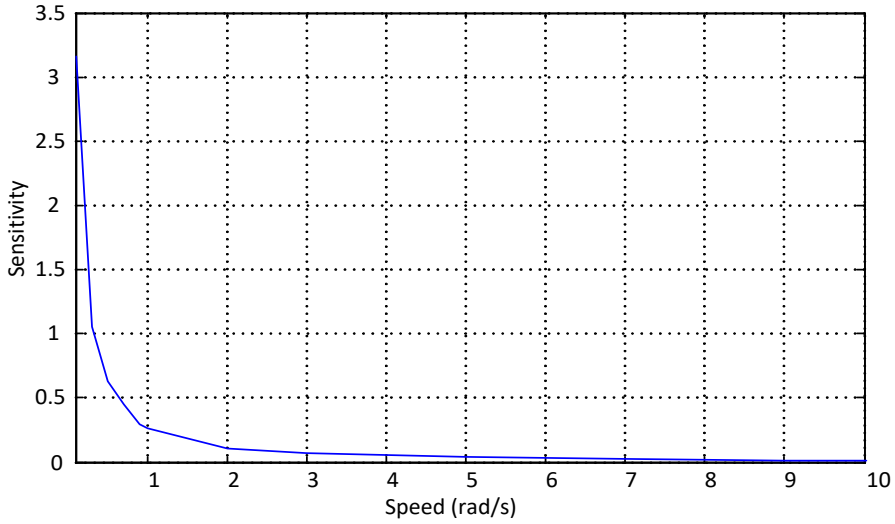

Fig. 7. Behaviour of $S_{\omega}^{R_s}$ for the first approach

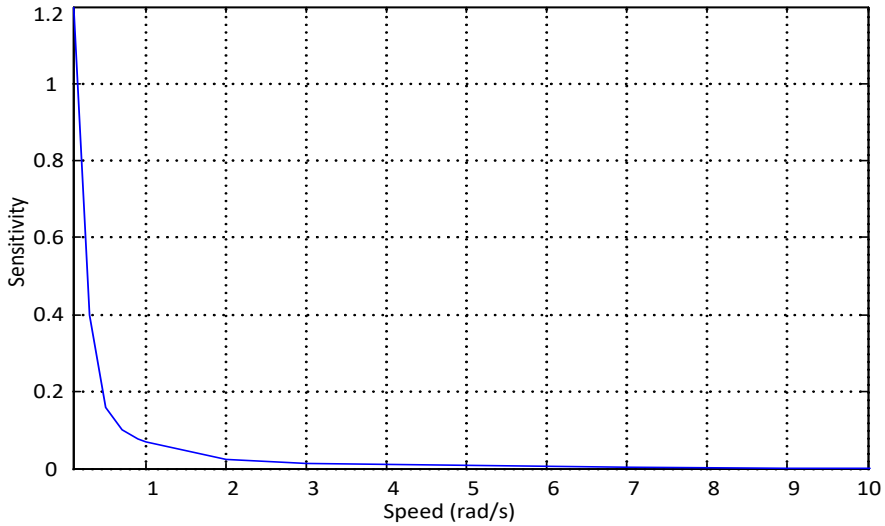

Fig. 8. Behaviour of $S_{\omega}^{R_s}$ for the second approach

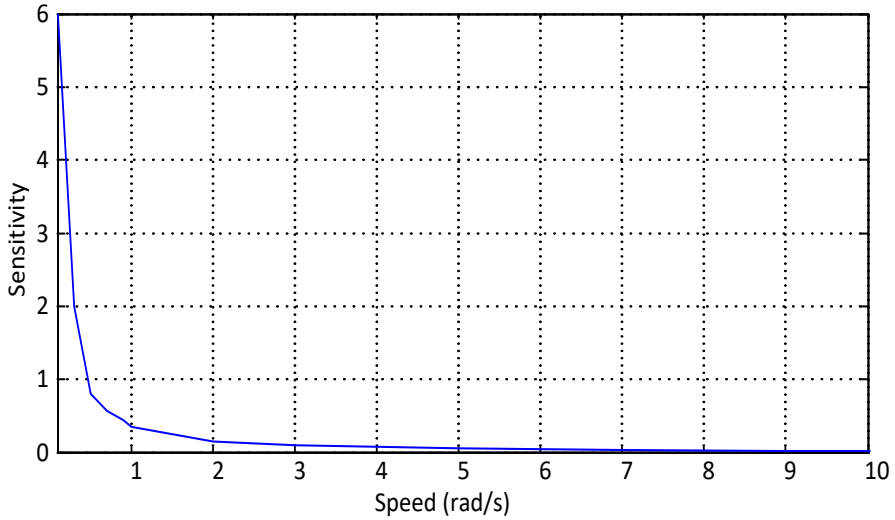

Fig. 9. Behaviour of $S_{\omega}^{L_s}$ for the first approach

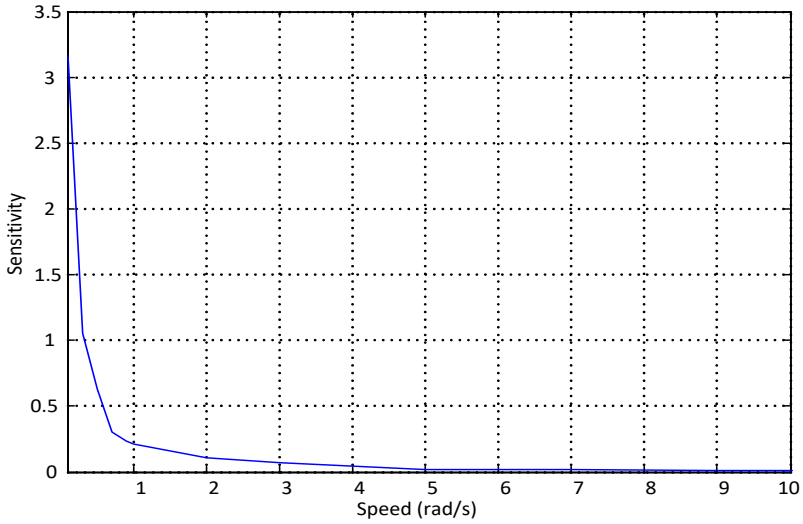

Fig. 10. Behaviour of S_{ω}^{Ls} for the second approach

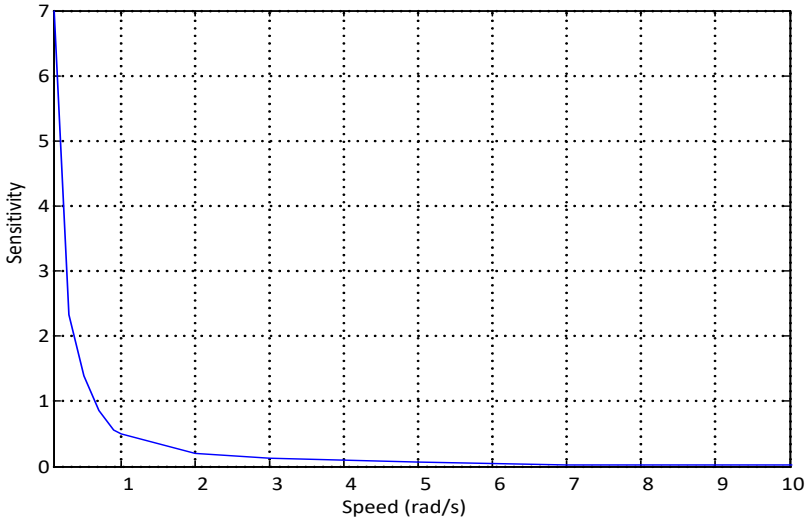

Fig. 11. Behaviour of $S_{\omega}^{\lambda mg}$ for the first approach

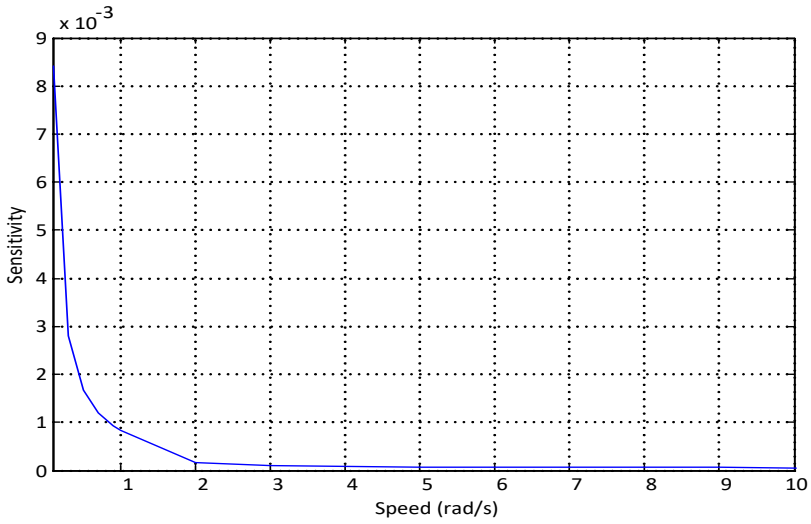

Fig. 12. Behaviour of $S_{\omega}^{\lambda mg}$ for the second approach

The following results show the performances of the two sensorless techniques under realistic residential/domestic load. During the tests we wanted to verify in particular the behavior of the two sensorless drives in two possible situations, corresponding respectively to the different positions in which the piston could be found at the moment the motor starts. This could in fact be found in two particular points: at the top (point B in Fig. 13) or at the bottom (point A). If the piston was located at A (Fig. 13–(a)), upon starting the motor should provide a sufficiently high torque to be able to compress the coolant contained inside the cylinder.

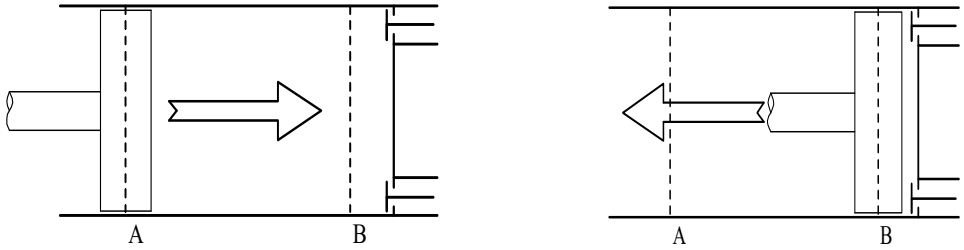

Fig. 13. The two different positions of the piston: (a) Compression, piston at A; (b) Suction, piston at B

Fig. 14 and Fig. 16 illustrate the profiles of actual, estimated and reference speeds and their relevant observation mismatch under realistic loading for the first and second semsorless approaches, respectively. As it can be noticed, the second sensorless provides better estimation accuracy thanks to the feedback correction made during the estimation of the EMF using corrective gains as presented in (21). Also, the speed under the second approach maintains successfully a good track of the reference irrespective of load variation. This fact not present in the first approach which gives priority to the second sensorless approach.

Fig. 15 and Fig. 17 show respectively the estimated and applied load torque on the motor outlining the compression and suction operating modes. For the two cases, the motor successfully developed a sufficient torque to drive the load which confirm the effectiveness of the adopted controller.

By observing Fig. 14 and Fig. 16, it can be revealed that the average speed estimation error for the first sensorless is 0.2 rad/s, meanwhile the average value of error under the second sensorless is nearly zero, which confirms the superiority of the second sensorless approach.

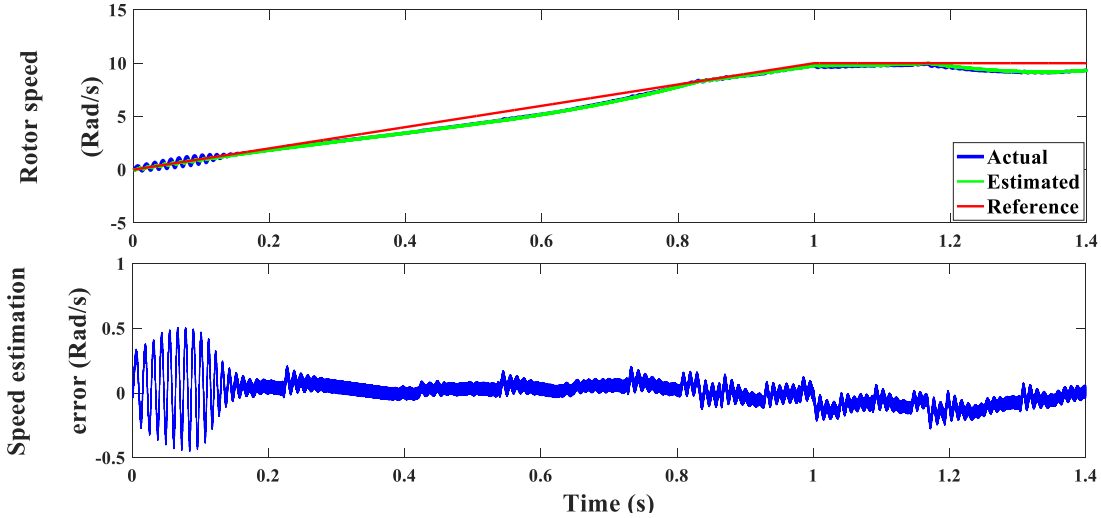

Fig. 14. Speed dynamic and estimation error for first sensorless

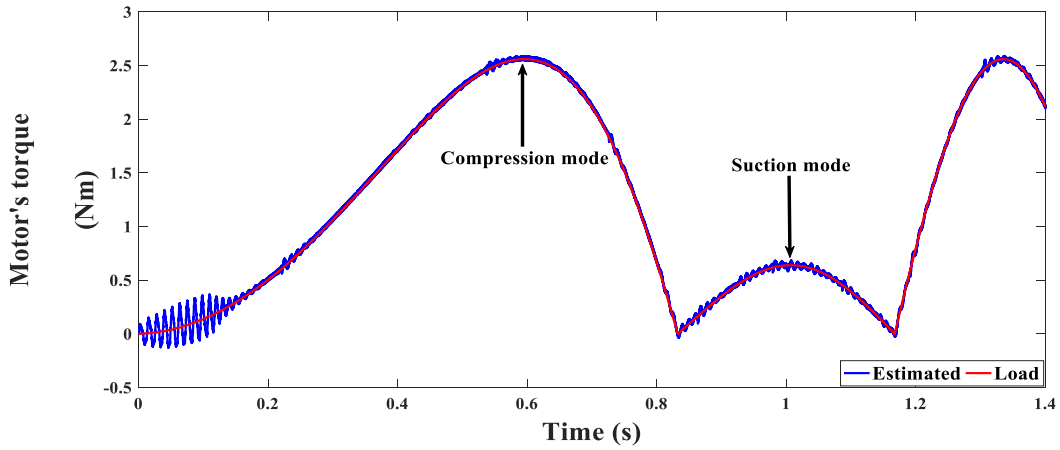

Fig. 15. Estimated and load torque applied under first sensorless

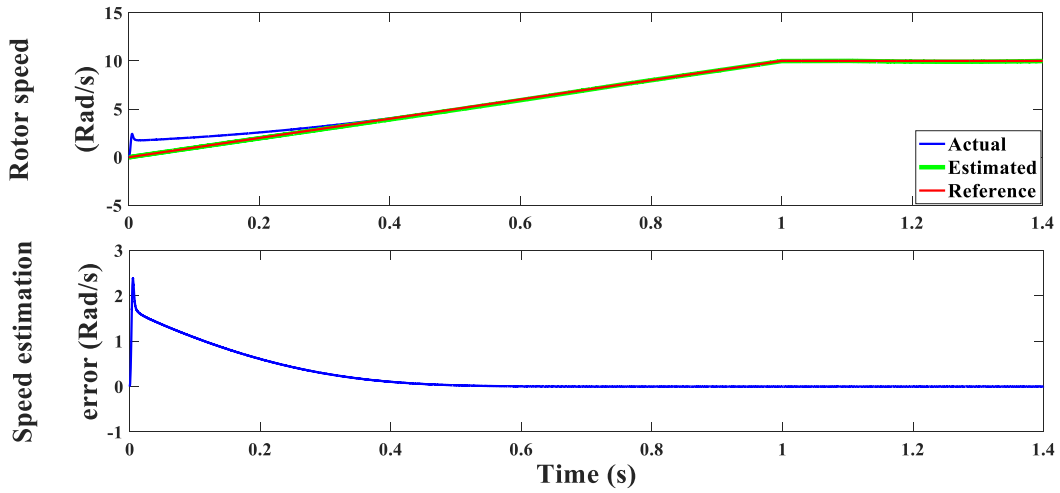

Fig. 16. Speed dynamic and estimation error for second sensorless

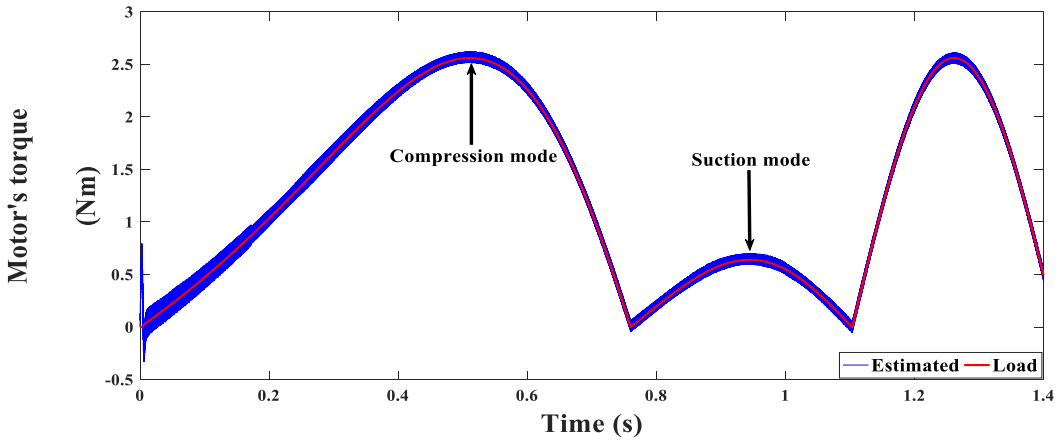

Fig. 17. Estimated and load torque applied under second snesorless

In order to give a detailed insight on the decoupling of active and reactive stator current components which validate the adopted control algorithm, Fig. 18 and Fig. 19 show respectively the d-q stator currents under the two sensorless schemes. As illustrated the d-current components follows the predefined zero value, meanwhile the q-current component follows the torque variation in appropriate manner.

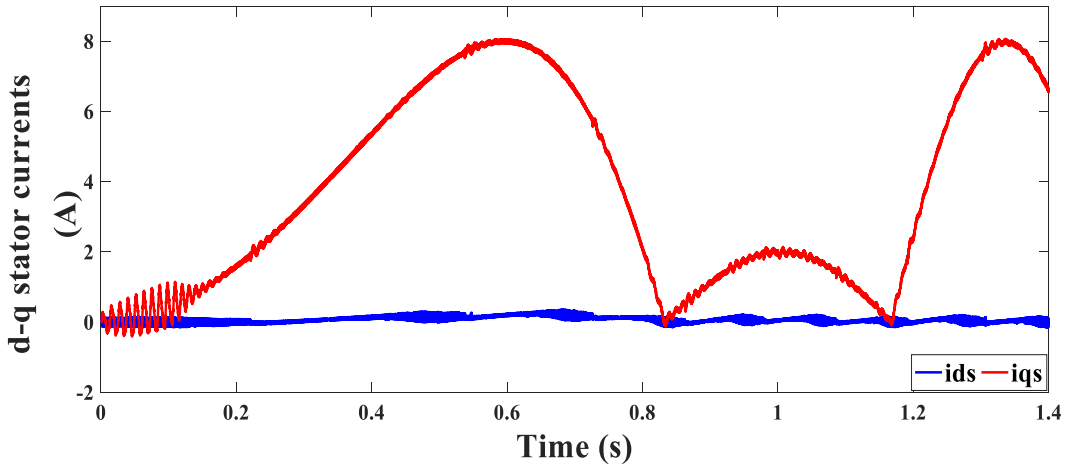

Fig. 18. d-q stator current under first sensorless technique

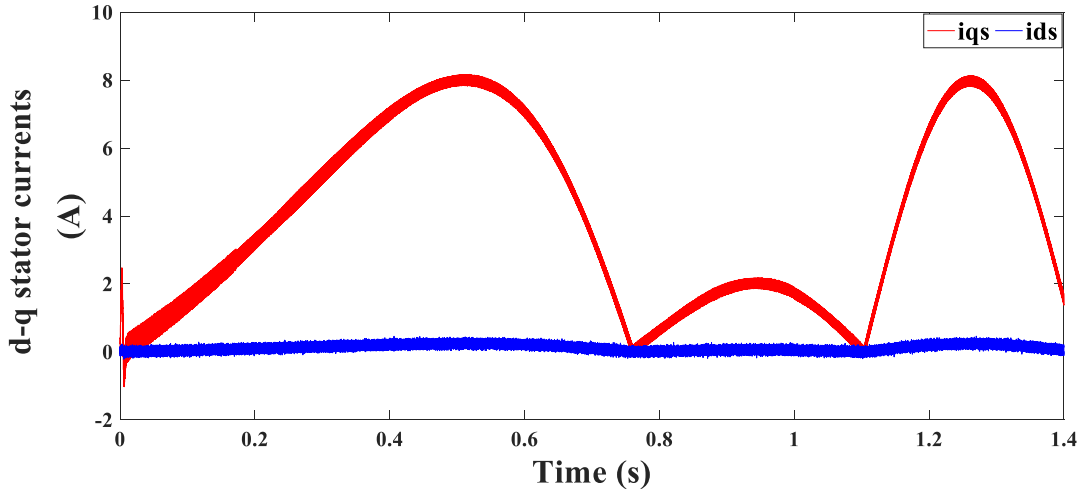

Fig. 19. d-q stator current under second sensorless technique

6. Conclusion

The study presented a thorough dynamic analysis for a PMSM drive used in residential applications while considering two different sensorless approaches. In the first sensorless technique, the speed is estimated by comparing two stator voltage values in two separate coordinates (actual and hypothesis). Meanwhile, in the second method, the rotor speed is evaluated by manipulating two motor current values defined in two rotating frames (actual and hypothesis). The theory of operation of the two sensorless methods is thoroughly explained. A comparative performance evaluation is considered to clarify the variations between the two sensorless methods considering the residential load profile while operating specifically at low-speed range. By attaining reduced estimation error and improved system robustness, the captured results demonstrate and validate the superiority of the current vector-based observer over the voltage vector-based observer. For future study, it is recommended to testify both sensing algorithms during different operating regimes such as field weakening operation while considering the same load profile.

Author Contribution: All authors contributed equally to the main contributor to this paper. All authors read and approved the final paper.

Funding: This research received no external funding.

Conflicts of Interest: The authors declare no conflict of interest.

Appendix

The overall system's parameters are summarized in Table A1.

Table A1. Overall system's parameters

Parameter	Value
Nominal torque	3.2 Nm
Nominal speed	377 Rad/s
R_s	750 mΩ
L_s	3 mH
λ_{mg}	0.215 Wb
J	8.26*10^{-4} kg.m^2
U_{dc}	160 V
Pole pairs (P)	1
(K_p,K_i) *for current regulators*	2.6 and 80
(K_{sp},K_{si}) and (K_e,K_θ)	(1,0.05) and (500,500)

References

[1] P. Lin, Z. Wu, K.-Z. Liu, and X.-M. Sun, "A class of linear–nonlinear switching active disturbance rejection speed and current controllers for PMSM," *IEEE Transactions on Power Electronics*, vol. 36, no. 12, pp. 14366–14382, Dec. 2021, https://doi.org/10.1109/TPEL.2021.3086273.

[2] J. Dilys and V. Stankevič, "A simple method for stator inductance and resistance estimation for PMSM at standstill," *International Journal of Robotics and Control Systems*, vol. 2, no. 3, pp. 477–491, 2022, https://doi.org/10.31763/ijrcs.v2i3.741.

[3] I.-C. Baik, K.-H. Kim, and M.-J. Youn, "Robust nonlinear speed control of PM synchronous motor using boundary layer integral sliding mode control technique," *IEEE Transactions on Control Systems Technology*, vol. 8, no. 1, pp. 47–54, Jan. 2000, https://doi.org/10.1109/87.817691.

[4] M. A. Mossa, O. Gam, N. Bianchi, and N. V. Quynh, "Enhanced control and power management for a renewable energy-based water pumping system," *IEEE Access*, vol. 10, pp. 36028–36056, 2022, https://doi.org/10.1109/ACCESS.2022.3163530.

[5] M. Azoma and M. Khan, "Recent advances in thermal management techniques for high-performance PMSMs—A comprehensive review," *Control Systems and Optimization Letters*, vol. 3, no. 3, pp. 360–369, 2025, https://doi.org/10.59247/csol.v3i3.180.

[6] M. A. Khan, "A review of analysis and existing simulation model of three-phase permanent magnet synchronous motor drive (PMSM)," *Control Systems and Optimization Letters*, vol. 2, no. 3, pp. 349–356, 2024, https://doi.org/10.59247/csol.v2i3.151.

[7] M. Azom and M. Khan, "Recent developments in control and simulation of permanent magnet synchronous motor systems," *Control Systems and Optimization Letters*, vol. 3, no. 1, pp. 84–91, 2025, https://doi.org/10.59247/csol.v3i1.173.

[8] M. Azom, M. Hossain, and M. Khan, "Review of electrical and thermal modeling techniques for three-phase PMSM drives," *Control Systems and Optimization Letters*, vol. 3, no. 1, pp. 75–83, 2025, https://doi.org/10.59247/csol.v3i1.172.

[9] M. Azom and M. Khan, "Challenges and advances in electrical and thermal modeling of high-precision PMSM drives," *Control Systems and Optimization Letters*, vol. 3, no. 2, pp. 130–137, 2025, https://doi.org/10.59247/csol.v3i2.175.

[10] W. Liang, W. Fei, and P. C.-K. Luk, "An improved sideband current harmonic model of interior PMSM drive by considering magnetic saturation and cross-coupling effects," *IEEE Transactions on Industrial Electronics*, vol. 63, no. 7, pp. 4097–4104, Jul. 2016, https://doi.org/10.1109/TIE.2016.2540585.

[11] A. A. Ahmed, A. Bakeer, H. H. Alhelou, P. Siano, and M. A. Mossa, "A new modulated finite control set-model predictive control of quasi-Z-source inverter for PMSM drives," *Electronics*, vol. 10, no. 22, 2021, https://doi.org/10.3390/electronics10222814.

[12] M. A. Mossa, O. Gam, and N. Bianchi, "Dynamic performance enhancement of a renewable energy system for grid connection and stand-alone operation with battery storage," *Energies*, vol. 15, no. 3, p. 1002, 2022, https://doi.org/10.3390/en15031002.

[13] O. Tola, E. Umoh, and E. Yahaya, "Pulse width modulation analysis of five-level inverter-fed permanent magnet synchronous motors for electric vehicle applications," *International Journal of Robotics and Control Systems*, vol. 1, no. 4, pp. 477–487, 2021, https://doi.org/10.31763/ijrcs.v1i4.483.

[14] O. Tola, E. Umoh, E. Yahaya, and O. Olusegun, "Permanent magnet synchronous generator connected to a grid via a high-speed sliding mode control," *International Journal of Robotics and Control Systems*, vol. 2, no. 2, pp. 379–395, 2022, https://doi.org/10.31763/ijrcs.v2i2.701.

[15] H. Mahmoud, M. A. Mohamed, A. A. Hassan, and M. A. Mossa, "A novel predictive voltage control technique for a grid-connected five-phase permanent magnet synchronous generator," *International Journal of Robotics and Control Systems*, vol. 4, no. 3, pp. 1158–1185, 2024, https://doi.org/10.31763/ijrcs.v4i3.1386.

[16] M. A. Mossa, T. Duc Do, A. Saad Al-Sumaiti, N. V. Quynh, and A. A. Z. Diab, "Effective model predictive voltage control for a sensorless doubly fed induction generator," *IEEE Canadian Journal of Electrical and Computer Engineering*, vol. 44, no. 1, pp. 50–64, 2021, https://doi.org/10.1109/ICJECE.2020.3018495.

[17] M. A. Mossa, M. K. Abdelhamid, and A. A. Hassan, "Enhancing the dynamic performance of a wind-driven grid-connected DFIG using an effective control approach," in *Proceedings of the IEEE Conference on Power Electronics and Renewable Energy (CPERE)*, Luxor, Egypt, 2023, pp. 1–7, https://doi.org/10.1109/CPERE56564.2023.10119614.

[18] Z. Dong, Z. Song, W. Wang, and C. Liu, "Improved zero-sequence current hysteresis control-based space vector modulation for open-end winding PMSM drives with common DC bus," *IEEE Transactions on Industrial Electronics*, vol. 70, no. 10, pp. 10755–10760, Oct. 2023, https://doi.org/10.1109/TIE.2022.3217600.

[19] M. A. Mossa, R. A. Mohamed, and A. S. Al-Sumaiti, "Performance enhancement of a grid-connected wind turbine-based PMSG using effective predictive control algorithm," *IEEE Access*, vol. 13, pp. 64160–64185, 2025, https://doi.org/10.1109/ACCESS.2025.3557194.

[20] H. Hamad Boughezala, K. Laroussi, S. Khadar, A. Saad Al-Sumaiti, and M. A. Mossa, "Optimized sensorless control of five-phase permanent magnet synchronous motor using a genetic algorithm—Real-time implementation," *IEEE Access*, vol. 12, pp. 98367–98378, 2024, https://doi.org/10.1109/ACCESS.2024.3429181.

[21] M. A. Mossa, O. Gam, and N. Bianchi, "Performance enhancement of a hybrid renewable energy system accompanied with energy storage unit using effective control system," *International Journal of Robotics and Control Systems*, vol. 2, no. 1, pp. 140–171, Feb. 2022, https://doi.org/10.31763/ijrcs.v2i1.599.

[22] M. A. Mossa, H. Echeikh, and A. Ma'arif, "Dynamic performance analysis of a five-phase PMSM drive using model reference adaptive system and enhanced sliding mode observer," *Journal of Robotics and Control*, vol. 3, no. 3, pp. 289–308, May 2022, https://doi.org/10.18196/jrc.v3i3.14632.

[23] Z. M. S. Elbarbary, O. K. Al-Harbi, S. F. Al-Gahtani, S. M. Irshad, A. Y. Abdelaziz, and M. A. Mossa, "Review of speed estimation algorithms for three-phase induction motor," *MethodsX*, vol. 12, p. 102546, 2024, https://doi.org/10.1016/j.mex.2024.102546.

[24] M. Konghirun and L. Xu, "A fast transient-current control strategy in sensorless vector-controlled permanent magnet synchronous motor," *IEEE Transactions on Power Electronics*, vol. 21, no. 5, pp. 1508–1512, Sep. 2006, https://doi.org/10.1109/TPEL.2006.882419.

[25] Y. Zhao, W. Qiao, and L. Wu, "Improved rotor position and speed estimators for sensorless control of interior permanent-magnet synchronous machines," *IEEE Journal of Emerging and Selected Topics in Power Electronics*, vol. 2, no. 3, pp. 627–639, Sep. 2014, https://doi.org/10.1109/JESTPE.2014.2298433.

[26] Q. An and L. Sun, "On-line parameter identification for vector-controlled PMSM drives using adaptive algorithm," in *Proceedings of the IEEE Vehicle Power and Propulsion Conference*, Harbin, China, 2008, pp. 1–6, https://doi.org/10.1109/VPPC.2008.4677634.

[27] Suryakant, M. Sreejeth, and M. Singh, "Sensorless control of PMSM drive with BEMF-based MRAC algorithm," in *Proceedings of the International Symposium on Advanced Electrical and Communication Technologies*, Rome, Italy, 2019, pp. 1–6, https://doi.org/10.1109/ISAECT47714.2019.9069705.

[28] A. Dianov, "An algorithm for estimation of stator resistance and inductance of low-cost SMPMSM drives," *IEEE Journal of Emerging and Selected Topics in Power Electronics*, vol. 10, no. 5, pp. 5626-5634, 2022, https://doi.org/10.1109/JESTPE.2022.3160154.

[29] M. Elnaggar, F. Aymen, and D. Mourad, "Sensorless speed estimation basing on MRAS model for a PMSM machine application," *International Journal of Robotics and Control Systems*, vol. 4, no. 4, pp. 1694–1711, 2024, https://doi.org/10.31763/ijrcs.v4i4.1585.

[30] Q. Li, X. Wang, J. Jiang, Q. Zhang, and Q. Tong, "Sensorless control for surface-mounted PM machine with a high inertial load," *CES Transactions on Electrical Machines and Systems*, vol. 2, no. 1, pp. 116–122, Mar. 2018, https://doi.org/10.23919/TEMS.2018.8326457.

[31] Z. Wang, Y. Zheng, Z. Zou, and M. Cheng, "Position sensorless control of interleaved CSI-fed PMSM drive with extended Kalman filter," *IEEE Transactions on Magnetics*, vol. 48, no. 11, pp. 3688–3691, Nov. 2012, https://doi.org/10.1109/TMAG.2012.2197180.

[32] Z. Yin, Y. Zhang, X. Cao, D. Yuan, and J. Liu, "Estimated position error suppression using novel PLL for IPMSM sensorless drives based on full-order SMO," *IEEE Transactions on Power Electronics*, vol. 37, no. 4, pp. 4463–4474, Apr. 2022, https://doi.org/10.1109/TPEL.2021.3125024.

[33] T. Liu, Z. Q. Zhu, Z.-Y. Wu, D. Stone, and M. Foster, "A simple sensorless position error correction method for dual three-phase permanent magnet synchronous machines," *IEEE Transactions on Energy Conversion*, vol. 36, no. 2, pp. 895–906, Jun. 2021, https://doi.org/10.1109/TEC.2020.3023904.

[34] K. Liu and Z. Q. Zhu, "Position offset-based parameter estimation for permanent magnet synchronous machines under variable speed control," *IEEE Transactions on Power Electronics*, vol. 30, no. 6, pp. 3438–3446, Jun. 2015, https://doi.org/10.1109/TPEL.2014.2337011.

[35] G. Wang, L. Ding, Z. Li, J. Xu, G. Zhang, H. Zhan, R. Ni, and D. Xu, "Enhanced position observer using second-order generalized integrator for sensorless interior permanent magnet synchronous motor drives," *IEEE Transactions on Energy Conversion*, vol. 29, no. 2, pp. 486–495, Jun. 2014, https://doi.org/10.1109/TEC.2014.2311098.

[36] A. Apte, V. A. Joshi, H. Mehta, and R. Walambe, "Disturbance-observer-based sensorless control of PMSM using integral state feedback controller," *IEEE Transactions on Power Electronics*, vol. 35, no. 6, pp. 6082–6090, Jun. 2020, https://doi.org/10.1109/TPEL.2019.2949921.

[37] J. Wang, Y. Liu, J. Yang, F. Wang, and J. Rodríguez, "Adaptive integral extended state observer-based improved multistep FCS-MPCC for PMSM," *IEEE Transactions on Power Electronics*, vol. 38, no. 9, pp. 11260–11276, Sep. 2023, https://doi.org/10.1109/TPEL.2023.3279856.

[38] K. Choi, Y. Kim, S.-K. Kim, and K.-S. Kim, "Current and position sensor fault diagnosis algorithm for PMSM drives based on robust state observer," *IEEE Transactions on Industrial Electronics*, vol. 68, no. 6, pp. 5227–5236, Jun. 2021, https://doi.org/10.1109/TIE.2020.2992977.

[39] H. Liu and S. Li, "Speed control for PMSM servo system using predictive functional control and extended state observer," *IEEE Transactions on Industrial Electronics*, vol. 59, no. 2, pp. 1171–1183, Feb. 2012, https://doi.org/10.1109/TIE.2011.2162217.

[40] K. C. Odo, S. V. Egoigwe, and C. U. Ogbuka, "A model-based PI controller tuning and design for field oriented current control of permanent magnet synchronous motor," *IOSR Journal of Electrical and Electronics Engineering*, vol. 14, no. 4, pp. 35–41, 2019, https://doi.org/10.9790/1676-1404023541.